Water Science and Engineering, 2013, 6(1): 78-90
doi:10.3882/j.issn.1674-2370.2013.01.006

http://www.waterjournal.cn
e-mail: wse2008@vip.163.com

Numerical simulation of slurry jets using mixture model

Wen-xin HUAI, Wan-yun XUE*, Zhong-dong QIAN

State Key Laboratory of Water Resources and Hydropower Engineering Science, Wuhan University, Wuhan 430072, P. R. China

Abstract: Slurry jets in a static uniform environment were simulated with a two-phase mixture model in which flow-particle interactions were considered. A standard k-ε turbulence model was chosen to close the governing equations. The computational results were in agreement with previous laboratory measurements. The characteristics of the two-phase flow field and the influences of hydraulic and geometric parameters on the distribution of the slurry jets were analyzed on the basis of the computational results. The calculated results reveal that if the initial velocity of the slurry jet is high, the jet spreads less in the radial direction. When the slurry jet is less influenced by the ambient fluid (when the Stokes number St is relatively large), the turbulent kinetic energy k and turbulent dissipation rate ε, which are relatively concentrated around the jet axis, decrease more rapidly after the slurry jet passes through the nozzle. For different values of St, the radial distributions of streamwise velocity and particle volume fraction are both self-similar and fit a Gaussian profile after the slurry jet fully develops. The decay rate of the particle velocity is lower than that of water velocity along the jet axis, and the axial distributions of the centerline particle streamwise velocity are self-similar along the jet axis. The pattern of particle dispersion depends on the Stokes number St. When St = 0.39, the particle dispersion along the radial direction is considerable, and the relative velocity is very low due to the low dynamic response time. When St = 3.08, the dispersion of particles along the radial direction is very little, and most of the particles have high relative velocities along the streamwise direction.

Key words: *slurry jet; numerical simulation; two-phase mixture model; Stokes number; flow-particle interaction*

1 Introduction

Turbulent slurry jets in liquids have a wide range of engineering applications in the fields of hydraulic engineering, chemical reaction, coal combustion, and environmental control. Due to the dynamic feedback between sediment and fluid phases, the fluid-sediment interaction is a very complex phenomenon, and the characteristics of the slurry jet are not completely known even for simple configurations.

A few studies of the two-phase flow characteristics of a slurry jet have been performed previously. Rajaratnam (1976) investigated single-phase jets which resulted from the discharge of a fluid with an initial momentum. When a sand phase is added to the single-phase jet, it is

This work was supported by the National Natural Science Foundation of China (Grant No. 11172218) and the Fundamental Research Funds for the Central Universities (Grant No. 2012206020209).
*Corresponding author (e-mail: *xuewanyun@126.com*)
Received Jan. 9, 2012; accepted Mar. 25, 2012

termed a two-phase jet. Singamsetti (1966) studied the dispersion of a downward round slurry jet based on the asymptotic invariance concept, and concluded that the velocity of the sand phase of two-phase jets followed a self-similar Gaussian distribution. Sun and Faeth (1986a, 1986b) and Sun et al. (1986) analyzed a two-phase slurry jet using a semi-empirical approach and concluded that the k-ε turbulence model was applicable to a wide range of multiphase flows. The structure of turbulent, diluted, particle-laden water jets submerged in still water was studied experimentally and theoretically by Parthasarathy and Faeth (1987). In their study, the following three limiting cases were examined: (1) locally homogeneous flow, where relative velocities between different phases were ignored; (2) deterministic separated flow, where relative velocities were considered, but particle-turbulence interactions were ignored; and (3) stochastic separated flow, where relative velocities and particle-turbulence interactions were both considered using the random-walk method. Jiang et al. (2005) used particle image velocimetry, combined with lower-density fluorescent hollow glass beads and polyamide particles to measure the velocities of sediment and fluid phases of a two-phase jet.

Numerical research of turbulent slurry jets has also been conducted. Dai et al. (1994) numerically simulated a three-dimensional spatially evolving, subsonic, plane jet with a large eddy simulation (LES) model. Their calculated mean velocity profiles were in agreement with experimental results, but the calculated self-similar turbulence intensities were distinctly higher than the experimental data. Lain and Garcia (2006) used so-called four-way coupling to investigate the influence of inter-particle collisions on the particle phase variables in the configuration of a free turbulent sediment-laden jet and found that the effects of inter-particle interactions were relevant to larger mass loading ratios due to the absence of walls confining the flow.

However, there have been few studies on particle dispersion and vortex structures in the vertical turbulent two-phase slurry jet. In this study, we used a two-phase mixture model to simulate two-dimensional vertical slurry jets in a static uniform environment. The flow field of the two phases, the particle dispersion patterns, and the turbulent kinetics of the jet were simulated. The self-similar criteria and the movement mechanisms of water and particles were studied.

2 Mathematical model

A two-phase mixture model was used in the simulation. It is assumed that the slurry jet flow consists of water and sediment phases, which are separate, and allows the phases to be interpenetrating. Therefore, the volume fractions of sediment and water phases for a control volume, φ_s and φ_f, can be equal to any value between 0 and 1, depending on the space occupied by the sediment phase and water phase. The mixture model also allows the two phases to move at different velocities, using the concept of slip velocities. The laws of conservation of mass and momentum are satisfied for the mixture. Coupling is achieved through pressure and interphasial exchange coefficients. The Syamlal-O'Brien drag model was used to describe the interaction between the two phases. Model details have been described by Fluent (2006).

2.1 Governing equations

The continuity equation of the mixture takes the form:

$$\frac{\partial \rho_{\mathrm{m}}}{\partial t}+\nabla\bullet\left(\rho_{\mathrm{m}}\boldsymbol{u}_{\mathrm{m}}\right)=0 \tag{1}$$

where ρ_{m} and $\boldsymbol{u}_{\mathrm{m}}$ are the mass density and mass-averaged velocity of the mixture, respectively. They can be expressed as

$$\rho_{\mathrm{m}}=\varphi_{\mathrm{f}}\rho_{\mathrm{f}}+\varphi_{\mathrm{s}}\rho_{\mathrm{s}} \tag{2}$$

$$\boldsymbol{u}_{\mathrm{m}}=\frac{1}{\rho_{\mathrm{m}}}\left(\varphi_{\mathrm{f}}\rho_{\mathrm{f}}\boldsymbol{u}_{\mathrm{f}}+\varphi_{\mathrm{s}}\rho_{\mathrm{s}}\boldsymbol{u}_{\mathrm{s}}\right) \tag{3}$$

where ρ_{s} and ρ_{f} are the mass densities of the sediment and water, respectively, and $\boldsymbol{u}_{\mathrm{s}}$ and $\boldsymbol{u}_{\mathrm{f}}$ are the velocities of the sediment and water, respectively.

The momentum equation for the mixture can be obtained by summing the individual momentum equations for water and sediment phases. It can be expressed as

$$\frac{\partial\left(\rho_{\mathrm{m}}\boldsymbol{u}_{\mathrm{m}}\right)}{\partial t}+\nabla\bullet\left(\rho_{\mathrm{m}}\boldsymbol{u}_{\mathrm{m}}\boldsymbol{u}_{\mathrm{m}}\right)=-\nabla p+\nabla\bullet\left(\boldsymbol{\tau}_{\mathrm{m}}+\boldsymbol{\tau}_{\mathrm{Tm}}\right)+\nabla\bullet\left(\varphi_{\mathrm{f}}\rho_{\mathrm{f}}\boldsymbol{u}_{\mathrm{df}}\boldsymbol{u}_{\mathrm{df}}+\varphi_{\mathrm{s}}\rho_{\mathrm{s}}\boldsymbol{u}_{\mathrm{ds}}\boldsymbol{u}_{\mathrm{ds}}\right)+\rho_{\mathrm{m}}\boldsymbol{g}+\boldsymbol{F} \tag{4}$$

where p is the pressure shared by the two phases; $\boldsymbol{\tau}_{\mathrm{m}}$ and $\boldsymbol{\tau}_{\mathrm{Tm}}$ represent the average viscous stress and turbulent stress, respectively; $\boldsymbol{g}$ is the gravitational acceleration; $\boldsymbol{F}$ is a body force; and $\boldsymbol{u}_{\mathrm{ds}}$ and $\boldsymbol{u}_{\mathrm{df}}$ are the drift velocities of the sediment and water, respectively. In this study, only one secondary phase (sediment) was present, so the drift velocity of sediment can be expressed as

$$\boldsymbol{u}_{\mathrm{ds}}=\left(1-\varphi_{\mathrm{s}}\right)\boldsymbol{u}_{\mathrm{sf}} \tag{5}$$

where $\boldsymbol{u}_{\mathrm{sf}}$ is the relative velocity (also referred to as the slip velocity), defined as the velocity of the secondary phase (sediment) relative to the velocity of the primary phase (water):

$$\boldsymbol{u}_{\mathrm{sf}}=\frac{\left(\rho_{\mathrm{s}}-\rho_{\mathrm{m}}\right)d_{\mathrm{s}}^{2}}{18\mu_{\mathrm{m}}f_{\mathrm{d}}}\left[\boldsymbol{g}-\left(\boldsymbol{u}_{\mathrm{m}}\bullet\nabla\right)\boldsymbol{u}_{\mathrm{m}}-\frac{\partial\boldsymbol{u}_{\mathrm{m}}}{\partial t}\right] \tag{6}$$

where d_{s} is the diameter of the particles of the secondary phase, and f_{d} is the default drag force, which can be expressed as

$$f_{\mathrm{d}}=\begin{cases}1+0.15Re^{0.687} & Re\le 1\ 000\\ 0.018\ 3Re & Re>1\ 000\end{cases} \tag{7}$$

where *Re* is the Reynolds number. Based on the continuity equation for the secondary phase, the volume fraction equation for the secondary phase can be obtained:

$$\frac{\partial\left(\varphi_{\mathrm{s}}\rho_{\mathrm{s}}\right)}{\partial t}+\nabla\bullet\left(\varphi_{\mathrm{s}}\rho_{\mathrm{s}}\boldsymbol{u}_{\mathrm{m}}\right)=-\nabla\bullet\left(\varphi_{\mathrm{s}}\rho_{\mathrm{s}}\boldsymbol{u}_{\mathrm{ds}}\right) \tag{8}$$

Since the volume fraction of particles is an important factor in the calculation of the effective viscosity for the mixture, the granular viscosity is used to get a value for the viscosity of the suspension. The volume-weighted average viscosity contains shear viscosity arising from particle momentum exchange due to translation and collision. The collisional and kinetic parts, and the optional frictional part, are added to give the dynamic viscosity of the sediment:

$$\mu_s = \mu_{sc} + \mu_{sk} + \mu_{sf} \tag{9}$$

where μ_{sc}, μ_{sk}, and μ_{sf} are collisional viscosity, kinetic viscosity, and frictional viscosity, respectively, and can be respectively expressed as

$$\mu_{sc} = \frac{4}{5}\varphi_s^2 \rho_s d_s g_{0s}(1+e_s)\left(\frac{\Theta_s}{\pi}\right)^{1/2} \tag{10}$$

$$\mu_{sk} = \frac{\varphi_s d_s \rho_s \sqrt{\Theta_s \pi}}{6(3-e_s)}\left[1+\frac{2}{5}(1+e_s)(3e_s-1)\varphi_s g_{0s}\right] \tag{11}$$

$$\mu_{sf} = \frac{P_s \sin\phi}{2\sqrt{I_{2D}}} \tag{12}$$

where g_{0s} is the radial distribution function, and $g_{0s} = \left[1-\left(\frac{\varphi_s}{\varphi_{smax}}\right)^{1/3}\right]^{-1}$, with φ_{smax} being the maximum value of φ_s, and $\varphi_{smax} = 0.63$; e_s is the restitution coefficient; Θ_s is the granular temperature; P_s is the sediment pressure, and $P_s = \varphi_s \rho_s \Theta_s + 2\rho_s(1+e_s)\varphi_s^2 g_{0s}\Theta_s$; I_{2D} is the second invariant of the deviatoric stress tensor; and ϕ is the internal friction angle.

2.2 Turbulent equations for mixture

Turbulent predictions for the mixture can be obtained using the standard k-ε model. The transport equations for the turbulent kinetic energy k and its rate of dissipation ε are expressed as

$$\frac{\partial(\rho_m k)}{\partial t} + \nabla\cdot(\rho_m \boldsymbol{u}_m k) = \nabla\cdot\left(\frac{\mu_{tm}}{\sigma_k}\nabla k\right) + G_{mk} - \rho_m \varepsilon \tag{13}$$

$$\frac{\partial(\rho_m \varepsilon)}{\partial t} + \nabla\cdot(\rho_m \boldsymbol{u}_m \varepsilon) = \nabla\cdot\left(\frac{\mu_{tm}}{\sigma_\varepsilon}\nabla \varepsilon\right) + \frac{\varepsilon}{k}(C_{1\varepsilon}G_{mk} - C_{2\varepsilon}\rho_m \varepsilon) \tag{14}$$

where G_{mk} is the production of turbulent kinetic energy; μ_{tm} is the turbulent viscosity, and $\mu_{tm} = \rho_m C_\mu k^2 / \varepsilon$; and C_μ, $C_{1\varepsilon}$, $C_{2\varepsilon}$, σ_k, and σ_ε are empirical constants: $C_\mu = 0.09$, $C_{1\varepsilon} = 1.44$, $C_{2\varepsilon} = 1.92$, $\sigma_k = 1.0$, and $\sigma_\varepsilon = 1.3$.

3 Experiments and computational conditions

Four laboratory experiments on slurry jets were originally conducted by Hall et al. (2010). In each experiment, the median particle size of sediment was $d_s = 0.206$ mm, the density of water was $\rho_f = 1\,000$ kg/m^3, and the density of particles was $\rho_s = 2\,545$ kg/m^3. The primary details of the slurry jet experiments are listed in Table 1, where d is the jet diameter at the nozzle, u_0 is the initial slurry jet velocity at the nozzle, φ_{s0} is the initial particle volume fraction, and *St* is the Stokes number. Fig. 1 shows the computational domain used in the present study, which mimicked the laboratory experiment above. On the basis of the axisymmetry of the flow field, two-dimensional numerical computations were conducted with the two-phase mixture model. The length and height of the computational domain were 2.5 m and 1.1 m, respectively. The impinging jet nozzle was located in the center of the upper side of

the tank and submerged just below the water surface.

Table1 Details of slurry jet experiments

Experiment No.	d (mm)	u_0 (m/s)	φ_{s0}	St
B1	15.5	1.00	0.055	0.39
B2	15.5	0.98	0.086	0.39
B3	15.5	0.98	0.124	0.39
C1	9.0	2.19	0.122	1.46

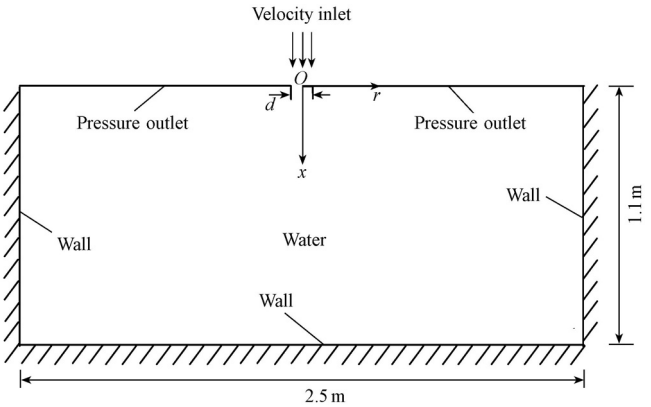

Fig. 1 Sketch of computational domain

Fig. 1 shows the boundary conditions. A velocity inlet boundary condition which was used to define the velocity and the scalar properties of the flow at inlet boundaries was applied at the flow inlet. The pressure outlet boundary conditions which required the specification of a static (gauge) pressure at the outlet boundary were used to model flow exits. Wall boundary conditions were applied on other sides of the tank. A two-dimensional non-uniform structured grid system with 140 000 elements was generated with the grid generator GAMBIT of the FLUENT package in the simulations.

4 Results

4.1 Verification of mathematical model

In a study of slurry jets, Fan et al. (2004) concluded that the Stokes number St is the main contributor to the distribution of water and particles. The Stokes number is defined as $St = \left[\rho d_s^2/(18\mu_f)\right]/(l_r/u_r)$, in which μ_f is the water dynamic viscosity; l_r is the characteristic length scale, and $l_r = d$; and u_r is the characteristic velocity scale, and $u_r = u_0$. The Stokes number St characterizes the extent to which the particles are influenced by the ambient fluid. Based on this, two representative computational results were selected. Fig. 2 shows the dispersion patterns of particles under a relatively great influence (St = 0.39) and relatively little influence (St = 1.46) after the slurry jet fully develops in the tank, about 15 seconds from the start of the jet.

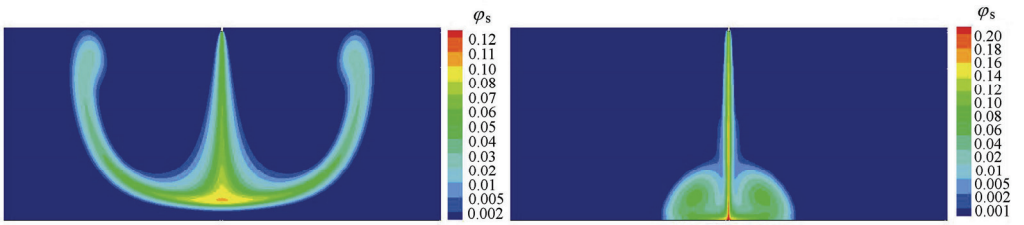

(a) St =0.39 (b) St =1.46

Fig. 2 Dispersion patterns of particles at different values of *St*

Profiles of particle volume fraction φ_s and streamwise velocity u_{mx} at different distances x from the water surface were simulated. The particle volume fraction profiles were normalized using the centerline particle volume fraction φ_{ms} and the length scale b_c where $\varphi_s/\varphi_{ms}=0.5$, and the streamwise velocity profiles were normalized using the centerline streamwise velocity u_{mcx} and the length scale b_v where $u_{mx}/u_{mcx}=0.5$. The normalized particle volume fraction and streamwise velocity profiles for the slurry jet experiment B3 are shown in Fig. 3 and Fig. 4, respectively. Fig. 3 and Fig. 4 show that the computational results agree with the experimental results, and the profiles of the normalized particle volume fraction and streamwise velocity are both self-similar; they are described by Eq. (15) and Eq. (16), respectively:

$$\frac{\varphi_s}{\varphi_{ms}}=e^{-0.75\left(\frac{r}{b_c}\right)^2} \tag{15}$$

$$\frac{u_{mx}}{u_{mcx}}=e^{-0.55\left(\frac{r}{b_v}\right)^2} \tag{16}$$

where r is the distance from the nozzle in the radial direction. However, there are some differences between computational and experimental streamwise velocity profiles in the ranges of r/b_v from −3.0 to −1.5 and from 1.5 to 3.0 due to the relatively low particle volume fraction and relatively strong turbulence.

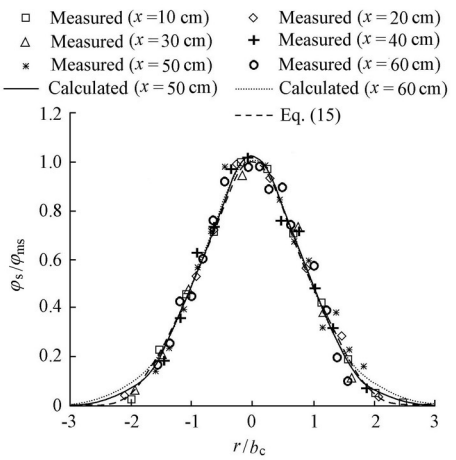

Fig. 3 Normalized particle volume fraction profiles

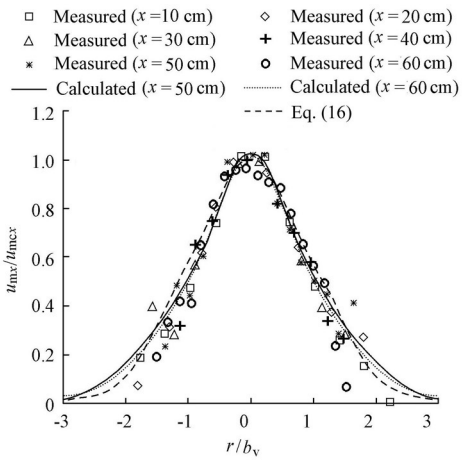

Fig. 4 Normalized streamwise velocity profiles

The half-width spreading of slurry jets is defined as a distance from the centerline to the radial location at which the particle volume fraction or streamwise velocity is one percent of the centerline particle volume fraction or streamwise velocity. Fig. 5 and Fig. 6 show the half-width spreading of particle volume fraction and streamwise velocity profiles of slurry jets. The computational results show a fair agreement with the experimental data.

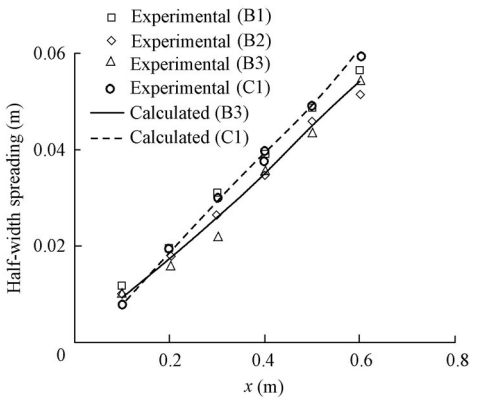

Fig. 5 Half-width spreading of particle volume fraction

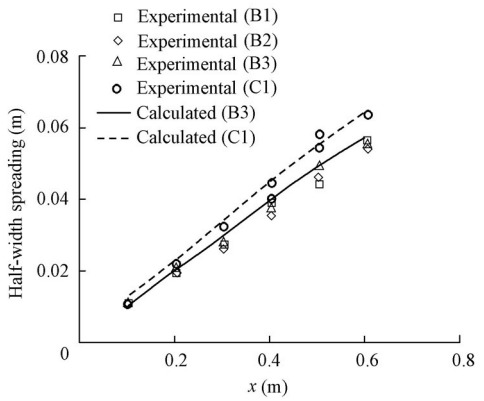

Fig. 6 Half-width spreading of streamwise velocity

4.2 Characteristics of flow field

Fig. 7 shows the velocity contours of jet flows with various Stokes numbers (St = 0.39 and St = 1.46) after the slurry jet fully develops. As the slurry jet flows out of the nozzle, the centerline velocity of the jet gradually decreases to zero owing to the resistance of water in the tank. Then the jet is divided into two parts that flow in opposite directions along the boundary of the deposition. The slurry jet is transformed to two symmetric flow recirculations and the locations of vortices are different for different values of St. Under a relatively little influence of the ambient fluid on particles (St = 1.46), the two vortices are relatively large and their centers are close to the lower side of the tank. In contrast, the vortices are not even found in Fig. 7(a) under a relatively large influence (St = 0.39). It can be seen from Fig. 7 that if the initial velocity of the slurry jet is high, the jet spreads less in the radial direction.

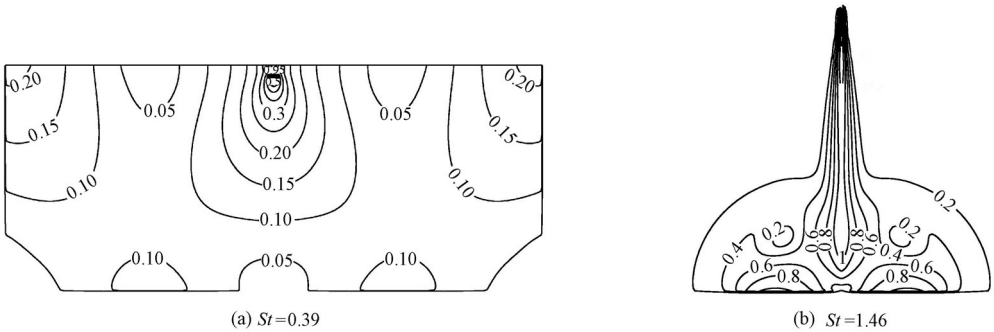

Fig. 7 Velocity contour of jet flows with different values of St (Unit: m/s)

Figs. 8 and 9 show the contours of the turbulent kinetic energy k and the turbulent dissipation rate ε in the tank for St = 0.39 and St = 1.46 after the slurry jet has fully developed, about 15 seconds from the start of the jet. The turbulent kinetic energy k and the turbulent dissipation rate ε decrease rapidly after the slurry jet flows out of the nozzle, with the decay rate higher than that of the jet velocity. The discharge of the jet flow gradually increases during the process of mixing with the ambient fluid after the slurry jet passes through the nozzle, and the jet velocity and turbulence intensity decrease with increasing discharge of the jet flow. It can be seen from Fig. 8 and Fig. 9 that, under a relatively large influence of the ambient fluid on particles (St = 0.39), the turbulent kinetic energy k and the turbulent dissipation rate ε are uniformly distributed in the tank. In contrast, under a relatively little influence (St = 1.46), the turbulent kinetic energy k and the turbulent dissipation rate ε are relatively concentrated around the jet axis and decrease more rapidly after the slurry jet passes through the nozzle.

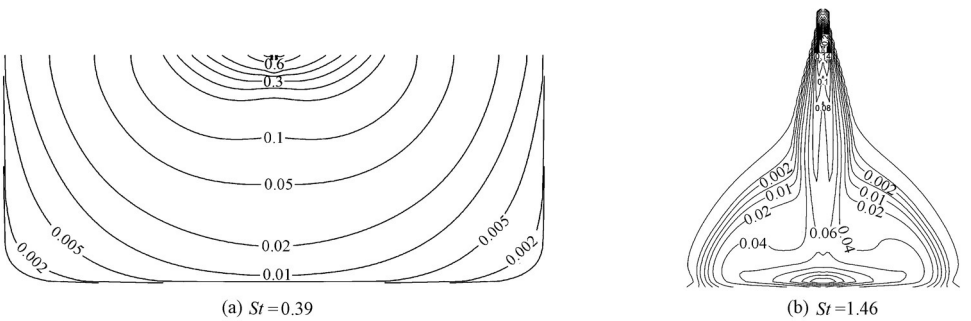

(a) St = 0.39 (b) St = 1.46

Fig. 8 Contours of turbulent kinetic energy k of jet flows with different values of St (Unit: m^2/s^2)

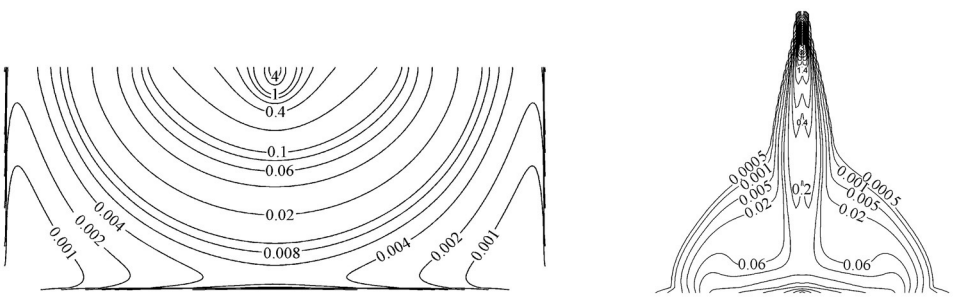

(a) St = 0.39 (b) St = 1.46

Fig. 9 Contours of turbulent dissipation rate ε of jet flows with different values of St (Unit: m^2/s^3)

4.3 Movement of particles

The velocity contours of particles with various Stokes numbers (St = 0.39 and St = 1.46) are shown in Fig. 10. As the slurry jet flows out of the nozzle, the velocity of the particle gradually decreases along the axial direction owing to the resistance of the ambient fluid. However, the decay rate of the particle velocity along the axial direction is less than that of the water velocity, owing to the settling velocity of the particle. When the particle velocity

becomes zero, most particles deposit on the ground owing to their submerged weight. Others spread out sideways and suspend owing to the turbulence of the fluid. As can be seen from these figures, when the slurry jet has a larger Stokes number, it spreads less radially.

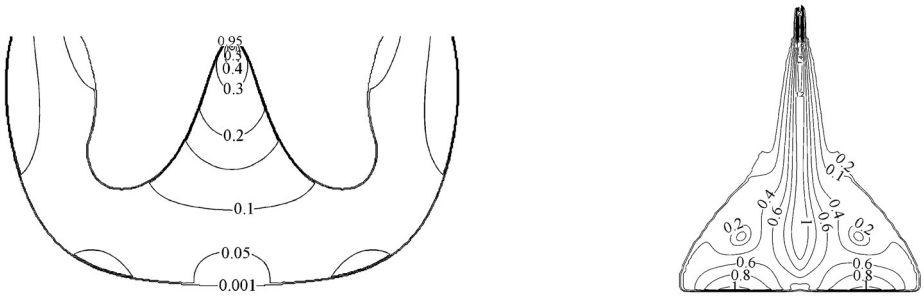

Fig. 10 Velocity contours of particles with different values of *St* (Unit: m/s)

To plot the data in a dimensionless form, dimensional considerations were used to predict the main characteristics of the jets (Hall et al 2010). Fig. 11 is a normalized plot of the centerline particle streamwise velocity for slurry jets, where the depth x is normalized by the length scale dFr (Fr is the Froude number), and u_{scx} is the centerline particle streamwise velocity of the slurry jet. As can be seen from Fig. 11, the computational results are in agreement with the experimental data, and the profiles of the normalized centerline particle streamwise velocity are self-similar and can be described by the following exponential equation:

$$\frac{u_{scx}Fr}{u_0}=\frac{3.4}{\left(\dfrac{x}{dFr}\right)^{1/2}+0.22} \tag{17}$$

The centerline particle streamwise velocity decreases rapidly near the nozzle, but it continues to decrease slightly far away from the nozzle and reaches a stable value at the end of the computational zone.

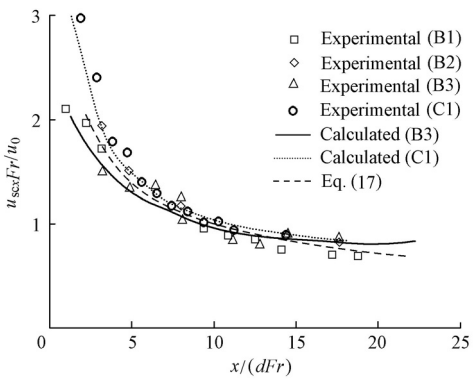

Fig. 11 Variations of normalized centerline particle streamwise velocity along axial direction for slurry jets

As can be seen from the verification of the mathematical model and analysis of computational data, the slurry jets were simulated well with the mixture model. However, the

influence of the Stokes number on the flow field and particle movement were not analyzed completely on the basis of the experimental results mentioned above, so another seven simulations of slurry jets were performed. In each simulation, the jet diameter at the nozzle, the median particle size of sediment, and the initial particle volume fraction were similar to the ones of the experiment B3, but the Stokes numbers for the seven slurry jets were different from that of the experiment B3 (St = 0.39); their values were 0.77, 1.15, 1.54, 1.92, 2.31, 2.69, and 3.08, respectively.

The dispersion patterns of particles for different Stokes numbers are depicted in Fig. 12, after the slurry jet has fully developed, about 15 seconds from the start of the jet. Fig. 12 shows that the dispersion pattern of particles depends on the Stokes number. As the Stokes number is relatively small, the recirculation region is relatively large, and the particle volume fraction within it is very small. In contrast, when the Stokes number is relatively large, the recirculation region is relatively small, and a large number of particles accumulate. When the Stokes number

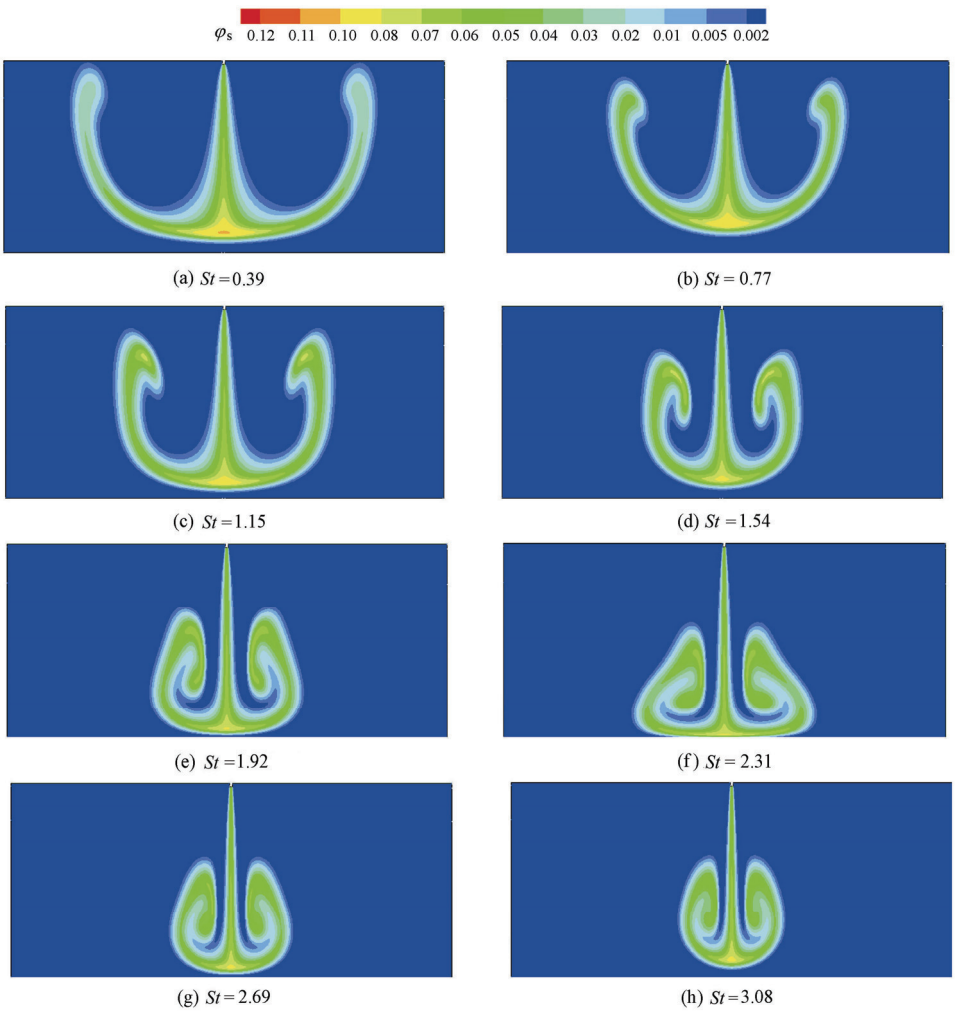

Fig. 12 Dispersion patterns of particles with different Stokes numbers

is as small as St = 0.39, particles follow the fluid closely because they can respond to the flow rapidly due to their very short dynamic response time. However, when the Stokes number increases to 3.08, the dispersion of particles along the radial direction is very little, and most of the particles penetrate the leading vortex structures and move downstream along nearly linear paths. The reason is that the dynamic response time of these particles is much longer than the characteristic time scale of the carrier fluid. As a result, the particles respond very slowly to the change in the flow field.

To explore the mechanisms of the particle dispersion described above, the relative velocity $\boldsymbol{u}_{\mathrm{sf}}$ (also referred to as the slip velocity) was computed. Fig. 13 shows the relative velocity fields of sediment for different Stokes numbers. When the Stokes number is low at a value of 0.39, the relative velocities have very small values and are distributed uniformly. This means that these particles can disperse almost as fast as water flows. When the Stokes numbers are as large as St = 3.08, only a few particles have large relative velocities along the radial direction

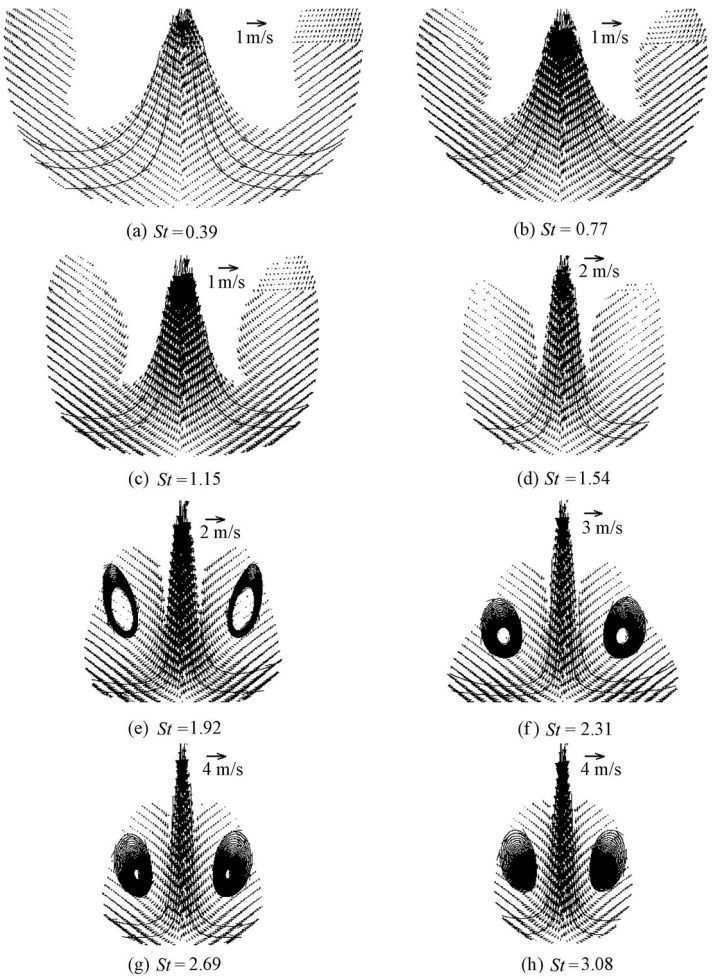

Fig. 13 Relative velocity fields of sediment for different Stokes numbers

and most of the particles have large relative velocities along the streamwise direction, showing that these particles disperse very little along the radial direction and mainly move downstream along a rectilinear path at high velocities. It seems that the relative velocity can reflect the dispersion mechanism of particles well.

5 Conclusions

Two-phase flow simulations of slurry jets in a static uniform environment were conducted using a mixture model in which the flow-particle interactions were considered and a standard k–ε turbulence model was chosen to close the governing equations. The mixture model, which also allows the two phases to move at different velocities using the concept of slip velocities, models fluid and particle phases by solving the continuity and momentum equations for the mixture, the volume fraction equations for the secondary phase, and algebraic expressions for the relative velocities. The following conclusions can be drawn:

(1) After the slurry jets fully develop in the tank, the computational results of the particle volume fraction and streamwise velocity agree with the experimental results, and the particle volume fraction and streamwise velocity profiles described by Eqs. (15) and (16) are both self-similar, but there are some differences between the computational and experimental streamwise velocity profiles in the ranges of r/b_v from −3.0 to −1.5 and from 1.5 to 3.0 due to the relatively low particle volume fraction and relatively strong turbulence. The half-width spreading of the particle volume fraction and streamwise velocity profiles of slurry jets shows a fair agreement between the computational results and the experimental data.

(2) The characteristics of flow fields of the two phases were analyzed on the basis of the computational results. If the initial velocity of the slurry jet is high, the jet spreads less in the radial direction. The turbulent kinetic energy k and the turbulent dissipation rate ε decrease rapidly after the slurry jet flows out of the nozzle, with the decay rate higher than that of the jet velocity. Under a relatively little influence of the ambient fluid on particles (when St is relatively large), the turbulent kinetic energy k and the turbulent dissipation rate ε are relatively concentrated around the jet axis and decrease more rapidly after the slurry jet passes through the nozzle.

(3) It was found that the decay rate of the particle velocity in the axial direction is less than that of the water velocity owing to the settling velocity of particles. The computational results of centerline particle streamwise velocities agree with the experimental data, and the profiles of centerline particle streamwise velocities described by Eq. (17) are self-similar. The pattern of particle dispersion depends on the Stokes number. When the Stokes number St = 0.39, particles follow the fluid closely and show considerable dispersion along the radial direction, and relative velocities have very small values and are distributed uniformly. When the Stokes number increases to 3.08, the dispersion of particles along the radial direction is very little, only a few particles have large relative velocities along the radial direction, and most of the particles have large relative velocities along the streamwise direction.

References

Dai, Y., Kobayashi, T., and Taniguchi, N. 1994. Large eddy simulation of plane turbulent jet flow using a new outflow velocity boundary condition. *JSME International Journal, Series B: Fluids and Thermal Engineering*, 37(2), 242-253.

Fan, J., Luo, K., Ha, M. Y., and Cen, K. 2004. Direct numerical simulation of a near-field particle-laden plane turbulent jet. *Physical Review E: Statistical, Nonlinear, and Soft Matter Physics*, 70(2), 026303. [doi:10.1103/PhysRevE.70.026303]

Fluent. 2006. *Fluent 6.3 User's Guide*. Lebanon: Fluent Inc.

Hall, N., Elenany, M., Zhu, D. Z., and Rajaratnam, N. 2010. Experimental study of sand and slurry jets in water. *Journal of Hydraulic Engineering*, 136(10), 727-738. [doi:10.1061/(ASCE)HY.1943-7900.0000235]

Jiang, J., Law, A. W. K., and Cheng, N. S. 2005. Two-phase analysis of vertical sediment-laden jets. *Journal of Engineering Mechanics*, 131(3), 308-318. [doi:10.1061/(ASCE)0733-9399(2005)131:3(308)]

Lain, S., and Garcia, J. A. 2006. Study of four-way coupling on turbulent particle-laden jet flows. *Chemical Engineering Science*, 61(20), 6775-6785. [doi:10.1016/j.ces.2006.07.005]

Parthasarathy, R. N., and Faeth, G. M. 1987. Structure of particle-laden turbulent water jets in still water. *International Journal of Multiphase Flow*, 13(5), 699-716. [doi:10.1016/0301-9322(87)90046-2]

Rajaratnam, N. 1976. *Turbulent Jets*. New York: Elsevier Science Ltd.

Singamsetti, S. R. 1966. Diffusion of sediment in a submerged jet. *Journal of the Hydraulics Divison*, 92(2), 153-168.

Sun, T. Y., and Faeth, G. M. 1986a. Structure of turbulent bubbly jets, I: Methods and centerline properties. *International Journal of Multiphase Flow*, 12(1), 99-114. [doi:10.1016/0301-9322(86)90006-6]

Sun, T. Y., and Faeth, G. M. 1986b. Structure of turbulent bubbly jets, II: Phase property profiles. *International Journal of Multiphase Flow*, 12(1), 115-126. [doi:10.1016/0301-9322(86)90007-8]

Sun, T. Y., Parthasarathy, R. N., and Faeth, G. M. 1986. Structure of bubbly round condensing jets. *Journal of Heat Transfer*, 108(4), 951-959. [doi:10.1115/1.3247040]

(Edited by Yan LEI)